Monolithic InP-Based Coherent 53 GHz Photodetector PIC with Integrated Polarization Rotator-Splitter

Hendrik Boerma[(1)], Trung Thanh Tran[(1)], Shahram Keyvaninia[(1)], Patrick Runge[(1)], Martin Schell[(1,2)]

[(1)] Fraunhofer Heinrich-Hertz-Institute, Einsteinufer 37, 10587 Berlin, Germany,
hendrik.boerma@hhi.fraunhofer.de
[(2)] Technical University Berlin, 10587 Berlin, Germany

Abstract *A high-speed monolithic InP-based coherent photodetector PIC with a responsivity of 0.05 A/W at 1550 nm for polarization- and phase-diverse detection is demonstrated. The monolithic integrated polarization-rotator-splitter enables a polarization extinction ratio of > 15 dB over the entire C-band. ©2023 The Author(s)*

Introduction

Polarization diverse modulation schemes allow doubling the transmission capacity of optical communication systems [1]. Therefore, coherent receivers with polarization de-multiplexing are widely deployed in long-haul communication networks [1]. Silicon photonic integrated circuits (PIC) with integrated polarization beam splitters (PBS) allow dual-polarization detection [2]. An advantage of InP-based high-speed coherent receiver PICs compared to silicon devices is the monolithic integration of the local oscillator [3], and a superior trade-off between responsivity and bandwidth. For this reason, next generation InP-based coherent photodetector PICs for 100 GBaud applications have been proposed recently [4, 5]. One of the major challenges for monolithic InP-based PICs is the integration of a polarization diversity circuit. Previous works on InP-based coherent photodetector PICs were based on active tuned asymmetric Mach-Zehnder interferometers using the width dependency of the birefringence [6]. Another approach applies plasmonic-based directional couplers with tight fabrication tolerances and additional loss [7].

A more recent approach is based on two steps: adiabatic TM_0 to TE_1 conversion and splitting of TE_1 and TE_0 into TE_0 into two different waveguides [8]. This polarization rotator-splitter (PRS) concept is based on mode-evolution and has an increased process tolerance [9]. In this contribution, a monolithic InP-based coherent photodetector PIC with an integrated PRS is demonstrated.

Chip Design and Fabrication

The PIC consists of two spot-size converters (SSC), a 3 dB-splitter, a PRS, two 90° hybrids, and eight photodiodes (PD) (Fig. 1). Because of etching the waveguide layer at the beginning of the spot size converter, the modes are confined in a broad rib waveguide enabling efficient coupling from a lensed fiber with a spot size of 3.5 µm. Due to an adiabatic taper the mode transforms from the chip facet mode into the higher confined waveguide mode. In the local oscillator (LO) path a 3 dB-coupler follows the SSC, splitting the LO light into the two 90° hybrids. The signal light coupled by the SSC into the waveguide is split, based on the states of polarization (SOP) by a monolithically integrated PRS. It consists of two parts: a mode converter and an asymmetric splitter. To enable a strong mode conversion effect vertical asymmetry of the waveguide is needed. Therefore, the same waveguide layers are used as presented in [10]. This enables an anti-crossing between the TM_0 and the TE_1 modes at a specific waveguide width. By adiabatically tapering the waveguide width through this point, it is possible to convert TM_0 into TE_1. The splitter is an asymmetric y-

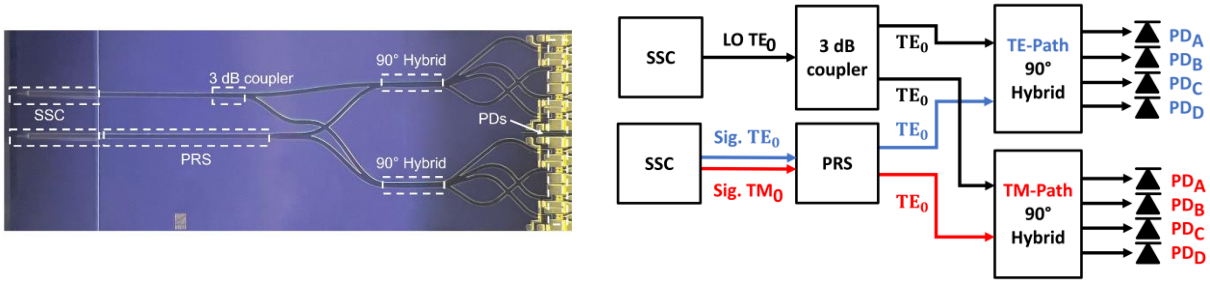

Fig. 1. Fabricated coherent photodetector PIC (left) and schematic of the coherent PIC (right)

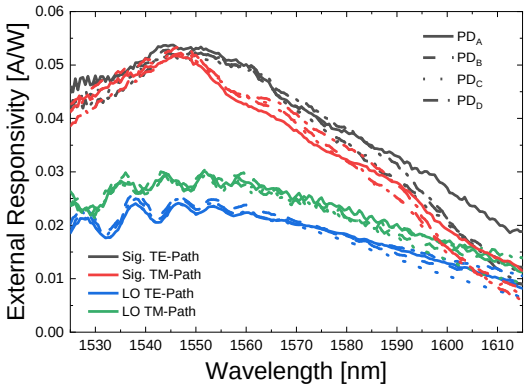

Fig. 2. Responsivity for all different channel combinations

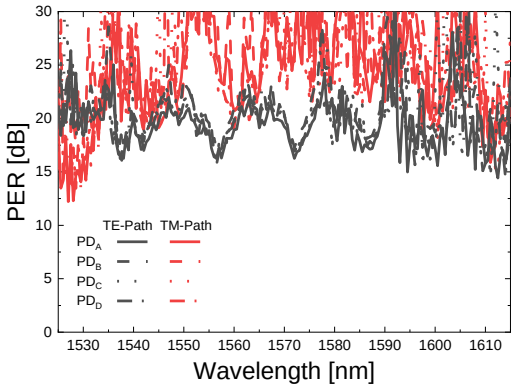

Fig. 3. PER for the two signal paths

branch with a gap width of 100 nm, splitting TE_0 and TE_1 into TE_0 modes of two different waveguides.

A major advantage of this scheme is the mode conversion of TM_0 to TE_0. This allows the LO SOP to be completely aligned to TE_0 to maximize the beating between the signal and the LO. The integrated 90° hybrids, realized as multimode interferometers, allow the IQ demodulation for both, the TE and the former TM path. The different optical signals are evanescently coupled into single-ended waveguide-integrated pin-photodiodes with an InGaAs absorption layer.

The PIC is fabricated on a 3-inch wafer. The epitaxial layers are grown by MOVPE. Contact photolithography combined with lift-off, dry and wet etching techniques is used to structure the majority of the doped photodiode and semi-insulating waveguide parts. An exception is the shallow etched waveguide, exposed by electron beam lithography to allow narrow gaps for the y-branches. Photoresist and SiN_x were used as protective layers during the etching processes. Electroplating formed the electrical contacts. The PIC has an anti-reflection coating to increase the coupling efficiency and to decrease reflections.

Measurement Results

The measurements of the responsivity, the polarization extinction ratio (PER), and the RF characteristics were carried out at a reverse bias voltage of 2V. Fig. 2 shows the external responsivity for the wavelength range of 1525 nm to 1615 nm. It reaches a maximum of above 0.05 A/W at 1550 nm for both signal paths. Due to the inherent 3-dB coupling loss, the LO paths have a TE responsivity of 0.02 A/W, showing an imbalance between the TE- and the TM-path. Since the 3-dB coupler has a symmetric design, this imbalance might arise from fabrication imperfections.

The PER was analyzed by measuring the dependence of the responsivity of the input polarization state with a polarization synthesizer. Fig. 3 shows the polarization extinction ratio for the TE and the TM signal path over a wavelength range from 1525 nm to 1615 nm. The PER is above 15 dB over the wavelength range from 1535 nm to 1605 nm. This large optical operation bandwidth follows from the adiabatic design of the PRS. An interesting fact to mention is that the LO path also exhibits a higher polarization-dependent loss (~10 dB at 1550 nm), due to the polarization-dependent design of the waveguides, enabling the polarization diversity

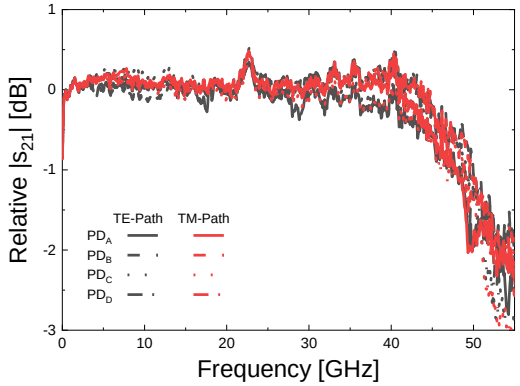

Fig. 4. Frequency response of the 8 photodiodes

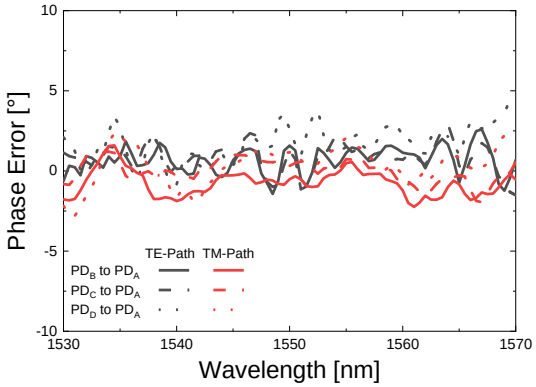

Fig. 5. Measured intra-symbol phase error for both paths

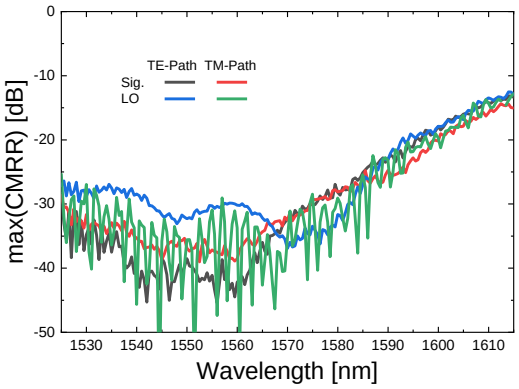

Fig. 6. DC CMRR for both paths

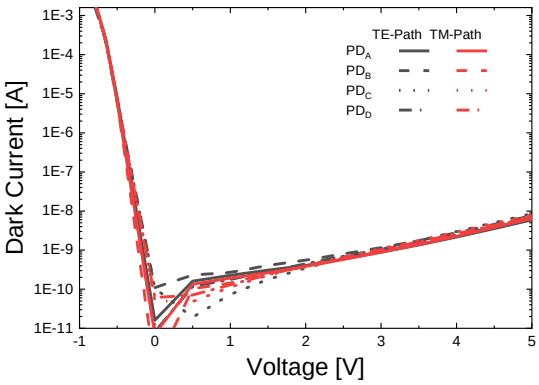

Fig. 7. Dark current of the 8 photodiodes

[10].

The RF transmission parameter $|s_{21}|$ was measured with a vector network analyzer combined with an optical modulator. The obtained 3 dB-bandwidth for all eight photodiodes is approximately 53 GHz (Fig. 4), limited by the electrical pad configuration rather than the photodiodes themselves. Fig. 5 shows the intra-symbol phase error. The phase error is below 5° for all channels over the wavelength range between 1530 nm to 1570 nm, showing the excellent behavior of the integrated 90° hybrids. The maximum common mode rejection ratio (CMRR) for both optical inputs and both polarization paths is shown in Fig. 6. The CMRR for all configurations is below -25 dB over the entire C-band. Fig. 7 shows the measurement of the PD current for different bias voltages without illumination, contributing to the noise behavior of the PIC. The photodiodes have a dark current below 1 nA for a reverse bias voltage of 2 V.

Conclusion

We demonstrate a monolithically integrated polarization- and phase-diverse coherent photodetector PIC based on InP. It has a responsivity of 0.05 A/W at 1550 nm, an electrical 3dB-bandwidth of 53 GHz, and a PER above 15 dB over the entire C-Band. The integrated PRS converts the TM_0 mode to TE_0, allowing the alignment of the LO to TE polarization. The presented device is a sophisticated example for the capability of monolithic polarization diversity integration into InP-based PICs.

While the PIC itself shows already good metrics, many characteristics leave room for further improvements. The size of the integrated PRS can be reduced by various waveguide optimization techniques, resulting in a reduced chip size and increased performance. The configuration of the electrical pads is a major contributor to the 3-dB bandwidth limitation at 53 GHz. By optimizing the pad configuration, we should be able to improve the bandwidth up to 70 GHz for 100 GBaud applications without sacrificing responsivity or any other performance metric. Another advancement would be the monolithic integration of the local oscillator into the PIC.

References

[1] K. Kikuchi, “Fundamentals of Coherent Optical Fiber Communications,” Journal of Lightwave Technology 34, 157-179 (2016), doi: 10.1109/JLT.2015.2463719.

[2] P. Dong X. Liu, S. Chandrasekhar, L. L. Buhl, R. Aroca, and Y. -K. Chen, “Monolithic Silicon Photonic Integrated Circuits for Compact 100 +Gb/s Coherent Optical Receivers and Transmitters,” IEEE Journal of Selected Topics in Quantum Electronics 20 (4), 150-157 (2014), doi: 10.1109/JSTQE.2013.2295181.

[3] S. Porto, M. Chitgarha, I. Leung, R. Maher, R. Going, S. Wolf, P. Studenkov, J. Zhang, H. Hodaei, T. Frost, H.-S. Tsai, S. Buggaveeti, A. Rashidinejad, A. Yekani, R. M. Nejad, M. Iglesias Olmedo, S. Kerns, J. Diniz, D. Pavinski, R. Brigham, B. Foo, M. Al-Khateeb, S. Koenig, P. Samra, M. Missey, V. Dominic, H. Sun, Steve Sanders, J. Osenbach, S. Corzine, P. Evans, Vikrant Lal, and M. Ziari, “Demonstration of a 2 × 800 Gb/s/wave Coherent Optical Engine Based on an InP Monolithic PIC,” Journal of Lightwave Technology 40, 664-671 (2022), doi: 10.1109/JLT.2021.3121284.

[4] P. Runge, G. Zhou, F. Ganzer, S. Seifert, S. Mutschall, and A. Seeger, “Polarisation Insensitive Coherent Receiver PIC for 100Gbaud Communication,” in Optical Fiber Communication Conference (OFC), OSA Technical Digest (Optical Society of America, 2016), paper Tu2D5, doi: 10.1364/OFC.2016.Tu2D.5.

[5] T. Okimoto, H. Yagi, K. Ebihara, K. Yamazaki, S. Okamoto, Y. Ohkura, K. Horino, K. Ashizawa, M. Ekawa, and Y. Yoneda, “InP-Based Butt-Joint Coupled Waveguide Photodiodes Integrated With Various Functions for 100 GBaud Coherent Detection,” IEEE Journal of Selected Topics in Quantum Electronics 28 (2), pp. 1-7 (2022), doi: 10.1364/OFC.2021.F2C.6

[6] R. Zhang, P. Runge, G. Zhou, R. Klötzer, D. Pech, H.-G. Bach, D. Pérez-Galacho, A. Ortega-Murnox, R. Halir, and, Í. Molina-Fernández, “56Gbaud DP-QPSK receiver module with a monolithic integrated PBS and 90° hybrid InP chip,” in 26th International Conference on Indium Phosphide and Related Materials (IEEE, 2014), pp. 1-2, doi: 10.1109/ICIPRM.2014.6880580.

[7] R. Kaiser, “Fabrication of polarization diversity heterodyne receiver PICs on InP: status, challenges and perspectives,” in Seventh International Conference on Indium Phosphide and Related Materials (IEEE, 1995), pp. 353-356, doi: 10.1109/ICIPRM.1995.522152.

[8] W. Yuan, K. Kojima, B. Wang, T. Koike-Akino, K. Parsons, S. Nishikawa, and E. Yagyu, “Mode-evolution-based polarization rotator-splitter design via simple fabrication process,” Optics Express 20 (9), 10163-10169 (2012), doi: 10.1364/OE.20.010163.

[9] S. Keyvaninia, H. Boerma, M. Wössner, F. Ganzer, P. Runge, and M. Schell, “Highly efficient passive InP polarization rotator-splitter,” Optics Express 29 (18), 25872-25881 (2019), doi: 10.1364/OE.27.025872.

[10] M. Perestjuk, H. Boerma, A. Schindler, S. Keyvaninia, P. Runge, and M. Schell, “Inverse-Designed InP-Based Polarization Rotator-Splitter,” in Optical Fiber Communication Conference, OSA Technical Digest (Optica Publishing Group, 2021), paper W6A49, doi: 10.1364/OFC.2021.W6A.49.